International Journal of Biological Macromolecules 83 (2016) 178–184

Contents lists available at ScienceDirect

International Journal of Biological Macromolecules

journal homepage: www.elsevier.com/locate/ijbiomac

Functional expression, monodispersity and conformational changes in the SBMV virus viral VPg on binding TFE

R.B. Mariutti[a], I.P. Caruso[b], A. Ullah[a], F.R. De Morais[b], D. Rehders[c], R.K. Arni[a,b,*]

[a] Multiuser Center for Biomolecular Innovation, IBILCE/UNESP, Brazil
[b] Department of Physics, IBILCE/UNESP, Brazil
[c] Laboratory for Structural Biology of Infection and Inflammation, Hamburg University, Germany

ARTICLE INFO

Article history:
Received 14 July 2015
Received in revised form 8 November 2015
Accepted 10 November 2015
Available online 22 November 2015

Keywords:
VPg
Viral genome-linked protein
Expression
Purification

ABSTRACT

Southern bean mosaic virus (SBMV) RNA purified from infected plants was used for cloning the viral genome-linked protein (VPg) and was subsequently expressed in *Escherichia coli*. Circular dichroism (CD), dynamic light scattering (DLS) and saturation transfer difference (STD) by nuclear magnetic resonance (NMR) measurements were employed to determine the degree of monodispersity and to investigate the conformational changes in the absence and presence of trifluoroethanol (TFE) which indicated increased helical content with increasing concentration of TFE. 8-Anilino-1-naphthalenesulfonic acid (ANS) was used as a probe to compare the unfolding regions of the protein before and after addition of TFE. The results indicated that although the TFE concentration influences VPg folding, it does not play a role in nucleotide binding and that the local solvent hydrophobicity causes significant conformational changes.

1. Introduction

Genome-linked viral proteins (VPgs) are involved in a number of processes ranging from replication to viral protein synthesis [1,2]. VPgs are small proteins that are covalently linked to the 5′ end of viral RNA via a phosphodiester bond formed between the hydroxyl groups of amino acid residues and the 5′ phosphate groups of RNA [3,4]. Often encountered in viruses with single-stranded positive-sense RNA (ssRNA) genomes, VPgs from fungal viruses, plant viruses and animal viruses with double or positive single strand (ssRNA) have been characterized [5,6]. VPgs from plant and animal viruses share many features, for example, they are products of polyprotein processing and are uridylated by their cognate RNA-dependent RNA polymerase (RdRP) [7–9] enabling VPgs to operate as primers during viral RNA synthesis. VPgs also share the presence of high percentages of basic amino acids (mostly lysine, glycine, threonine and arginine) contributing to the interaction with the negatively charged RNA [10]. The covalent binding of VPgs to RNAs exhibits some differences; picornaviruses, potyviruses and caliciviruses use the hydroxyl group of a tyrosine residue whereas comoviruses and nepovirus are reported to use a serine residue [6]. Threonine also contains a hydroxyl group, but the only evidence that it is used for RNA binding was reported by [11] when investigating VPg from SBMV covalently attached to genomic RNAs. VPg from sobemovirus is a cleavage product of its precursor polyprotein (VPg-proteinase-polymerase) [12] and the residue for RNA binding is not conserved within its genre [13]. All positive-sense ssRNA viruses that infect mammalian, insect or plant cells replicate in association with host endomembrane [14] and different host factors may influence the process [15,16]. Some phytoviral (*Sesbania mosaic virus*; *Potato virus A*, *Potato virus Y*, *Lettuce mosaic virus*, and *Rice yellow mottle virus*) VPgs were shown to be natively unfolded proteins [17–20] and hence recalcitrant for crystallization. Therefore, to date, not a single crystal structure of these proteins has been determined. Nevertheless, the crystal structures of synthetic peptides corresponding to *Picornaviridae* VPgs (<3 kDa) (PDB: 2D7S, 4IKA, 3CDW) complexed with their cognate RdRP indicate that the peptides are almost completely random coiled without any alpha helix or beta strand. More recently, the solution structure of recombinant VPg from *Caliciviridae* (PDB: 2MXD) has been elucidated [21].

In the present study, VPg from SBMV was expressed in *Escherichia coli* and purified. Circular dichroism (CD) was employed to assess the VPg secondary structure conformational content and its variation in the presence of increasing concentrations of reagents that mimic membrane environments

* Corresponding author at: Multiuser Center for Biomolecular Innovation, Universidade Estadual Paulista (UNESP), São Jose do Rio Preto, 15054-000 SP, Brazil.
E-mail address: arni@sjrp.unesp.br (R.K. Arni).

http://dx.doi.org/10.1016/j.ijbiomac.2015.11.026
0141-8130/

(2,2,2-trifluoroetahnol, TFE). Far UV-CD spectra and 8-anilino-1-naphthalenesulfonic acid (ANS) were used to compare the unfolded regions of the protein before and after the addition of TFE and saturation transfer difference by nuclear magnetic resonance (STD-NMR) spectroscopy was employed to compare the binding pattern between the VPg from SBMV and dNTPs, to gain insights into molecular recognition of different nucleotides by VPg.

2. Methods

2.1. Virus purification and RNA extraction

The virus was purified from infected leaves of *Phaseolus vulgaris* following the method of [22]. Viral RNA was extracted using the RNeasy Plant Mini Kit (Qiagen) following the manufacturer's instructions.

2.2. Primer design, cDNA syntheses and PCR amplification of the ORF1

Primers were designed as shown below to amplify the sequence that encodes VPg from genomic RNA of an isolate of SBMV. *Bam*HI and *Xho*I restriction sites were incorporated in the forward and reverse primers, respectively, to facilitate cloning in pET28a expression vector. A TEV protease cleavage site was also incorporated in the forward primer to permit cleavage of the hexahistidine tag of the recombinant protein after purification.

Forward primer: 5′-GGATCC**GGTGAAAATTTATATTTTCAA**GGTACTCTACCT CCTGATCTGTCCG-3′ (*Bam*HI restriction site underlined and TEV cleavage site in bold).

Reverse primer: 5′-CTCGAGTCATTCCTGAGCTGAAGTCCA-3′ (*Xho*I restriction site underlined).

First strand cDNA was synthesized using Superscript II Reverse Transcriptase (Invitrogen). Polymerase chain reaction (PCR) was performed for the amplification of the sequence that encodes VPg in 100 μL mixture containing 50 ng of genomic RNA, 1 μL (10 μM) of each primer, 2 μL (10 mM) dNTPs, 10 μL of PCR buffer (100 mM Tris–HCl, pH 8.8, 500 mM KCl, 0.8% Nonidet P40, and 25 mM $MgCl_2$), and 2.5 U of native *Taq* DNA polymerase enzyme (MBI Fermentas). The reaction was carried out using the following reaction cycles in a programmable thermocycler (Eppendorf): initial denaturation at 95 °C for 10 min followed by 30 consecutive cycles of denaturation at 95 °C for 30 s, annealing for 1 min at 55 °C, extension at 72 °C for 1 min 30 s, followed by a final extension at 72 °C for 10 min. The amplification product was analyzed by electrophoresis on a 1% agarose gel stained with ethidium bromide. The specific PCR product obtained was purified using PCR gel purification kit (Qiagen) and the product was used for ligation in pGEM-T Easy vector.

2.3. Cloning in pGEM-T easy vector

In order to clone the sequence that encodes VPg, pGEM-T Easy vector (Promega) was used. The resulting PCR product and pGEM-T Easy vector were ligated overnight at 4 °C using T4 DNA ligase. This construct was transformed into *E. coli* DH5α cells and the resulting colonies were screened by blue white colony selection and PCR. One clone was used to plasmid extraction and it was sequenced by automatic sequencer ABI 377 DNA Sequencer.

2.4. Cloning in pET28a

The sequence cloned in pGEM-T Easy vector was digested with *Bam*HI and *Xho*I restriction enzymes and analyzed on a 1% agarose gel. A 300 bp insert (ORF) was purified from the agarose gel by using a gel extraction and purification kit (Qiagen) and cloned in pET28a vector (Novagen). Positive clones were first selected by PCR and reconfirmed by restriction digestion.

2.5. Expression of recombinant VPg in E. coli using pET28a vector

For expression, VPg protein was tagged with 6xHis; *E. coli* cells BL21-CodonPlus®-RIL were transformed with the pET28a construct and incubated in LB broth (with 0.2% glucose and 34 μg/ml kanamycin for selection). The medium was inoculated with an overnight culture (1:100 dilution) and the culture was incubated under agitation at 30 °C until an OD_{600} of ~0.5 was attained. Subsequently, 0.2 mM IPTG was added and the culture was further incubated at 18 °C for 16 h.

2.6. Protein purification

2.6.1. Purification of the VPg 6xHis recombinant protein

Cells were harvested by centrifugation at 6000 × *g*, at 4 °C for 20 min and lysed in buffer 20 mM sodium phosphate pH 7.4, 200 mM NaCl (buffer A) by sonication on ice. The clear supernatant obtained by centrifugation at 15,000 × *g* for 45 min (4 °C) was subsequently applied onto a nickel resin column pre-equilibrated with buffer A. The column was washed with buffer A which additionally contained 70 mM imidazole and the recombinant protein was eluted with buffer A which contained 400 mM imidazole, concentrated and subjected to a final step of molecular exclusion chromatography by utilizing a Superdex G75/300 GE column. The purity of VPg throughout *E. coli* expression and purification steps was determined by SDS-PAGE.

2.7. Dynamic light scattering

DLS measurements were carried out using freshly prepared samples in buffer 20 mM sodium phosphate pH 7.5, 100 mM NaCl. Each experiment was carried out in a quartz cuvette with an optical path length of 3 mm at 25 °C and the results presented are the average values obtained from 20 scans. The experiments were repeated at different pHs in the presence of salts, amino acids, sugars, detergents, reducing agents and also in the presence of possible ligands, such as, dATP, dUTP, dGTP and dCTP (Table 1).

2.8. Circular dichroism spectroscopy

Far UV-CD spectra were recorded at room temperature (25 °C) on a Jasco J-710 Spectropolarimeter (Jasco, Tokyo, Japan) and quartz cells with a path length of 0.5 mm. CD spectra were recorded in the 190–260 nm range at a scan rate 50 nm/min, response time of 1.0 s, spectral bandwidth of 1.0 nm and spectral resolution of 0.1 nm. For each spectrum, 7 accumulations were performed. The VPg concentration was maintained constant at 30 μM during all experiments. The addition of 2,2,2-trifluoroethanol (TFE, Sigma) was performed in the 0–30% range with an increment of 10% (v/v). All spectra were corrected by subtraction of the respective buffer spectra. Secondary structure percentages for each tested condition were calculated with CONTINLL software of CDPro package, using the reference set of proteins SMP56 [23].

2.9. Binding of probe 8-aniline-1-naphthalene sulfonate (ANS)

The fluorescence measurements were performed at room temperature (25 °C) by using an ISS PC1 steady-state Spectrofluorimeter (Champaign, IL, USA) equipped with quartz cells of 10 mm path lengths. Both excitation and emission bandwidths were set at 8 nm. The excitation wavelength at 370 nm was chosen since it only causes excitation of ANS. The emission spectrum was collected in the range of 390–700 nm with an increment of 1 nm and each point

Table 1
Reagents used to investigate the aggregation state of recombinant VPg.

	Reagents	Concentration range
Salts	NaCl	0–1 M
	KCl	0–1 M
	NaF	0–500 mM
	NaCl + KCl	0–500 mM
	$CaCl_2$	0–200 mM
	$MgCl_2$	0–200 mM
	$MgSO_4$	0–400 mM
	Urea	0–500 mM
Amino acids	Glycine	0.5–2%
	L-Arginine	0–0.5 M
Genetic material	Oligonucleotides	0.1–100 μM
	Nucleotides (dNTPs)	0–0.5 mM
	β-Cyclodextrin	0–100 mM
Sugars and alcohols	Sucrose	0–1 M
	Glucose	0–1 M
	Sorbitol	0–40%
	Glycerol	5–40%
	Trifluoroethanol	5–30%
	Ethanol	0–5%
Detergents	Triton X-100	0–0.02%
	Tween 20	0–0.1%
	CHAPS	0–0.5%
	NP-40	0–0.2%
Reducing agents	DTT	0–20 mM
	2-Mercaptoethanol	0–10 mM

in the emission spectrum is the average of 10 accumulations. The ANS binding probe (250 μM) to VPg (100 μM) was monitored both in the absence and presence of 30% TFE (vol:vol). As a reference spectrum, the ANS emission was also analyzed in a buffer solution in the absence and presence of 30% TFE.

2.10. Prediction of intrinsic disorder in VPg

VPg amino acid sequence was analyzed using computational predictor software FoldIndex© tool to identify ordered and disordered regions within the protein. The intrinsic disorder in VPg and the structural changes induced by TFE were evaluated.

2.11. Saturation transfer difference nuclear magnetic resonance spectroscopy

NMR experiments were performed on a Brucker AVANCE III HD 600 MHz NMR spectrometer equipped with a triple-resonance cryoprobe. The protein concentration was adjusted to 15 μM in a 50 mM deuterated phosphate buffer pH 7.5 and the ligand concentration was 300 μM. Saturation transfer difference NMR spectroscopy [24] experiments were carried out using the standard *stddiffesgp*.3 pulse sequence at 393 K, where protein signal suppression is performed by a spin-lock filter. For protein saturation, on-resonance radiation was set to +300 Hz and off-resonance to +24,000 Hz. Control experiments were performed under identical conditions in the absence of protein. To check whether conformational changes can impair binding, experiments were also carried out in the presence of 30% TFE under identical conditions.

Group epitope mapping was performed by comparing off-resonance and difference spectra and adjusting the relative signal intensities in the calculation of the STD amplification factor (STD-AF) following the equation:

$$\text{STD-AF} = \frac{I_{\text{off-resonance}} - I_{\text{on-resonance}}}{I_{\text{off-resonance}}}$$

The largest STD-AF is associated to 100% relative STD effect, and the others signals are compared to it. Higher STD-AF is associated to closer contact to protein atoms since the Nuclear Overhauser

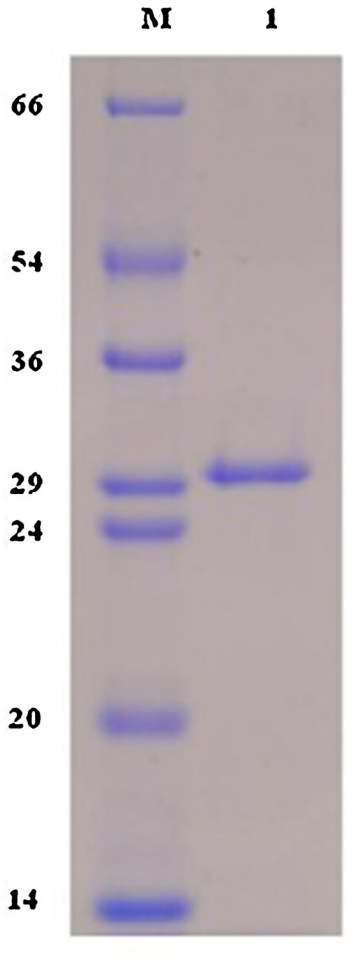

Fig. 1. SDS-PAGE 12% gel of viral particles obtained from infected bean leaves: lane (M), molecular-weight markers (labelled in kDa); lane (1), represents purified SBMV.

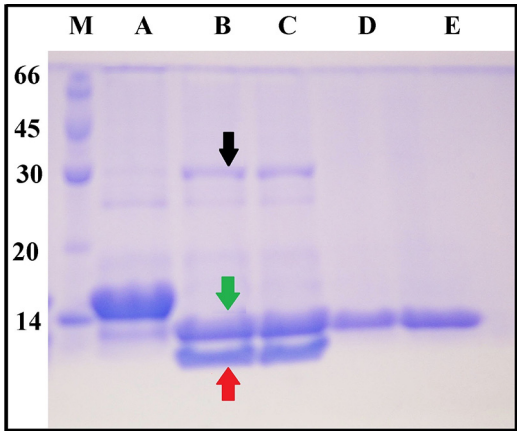

Fig. 2. SDS-PAGE analysis of purified VPg. Lane (M), molecular-weight markers (labelled in kDa). (A) tagged, purified VPg. (B) and (C) tagged VPg after 8 and 16 h of digestion using TEV protease. The black arrow indicates TEV protease, green arrow indicates untagged VPg and red arrow the tag. (D) Untagged VPg isolated. (E) 1 μL of VPg concentrated to 10 mg/mL. (For interpretation of the references to colour in this figure legend, the reader is referred to the web version of this article.)

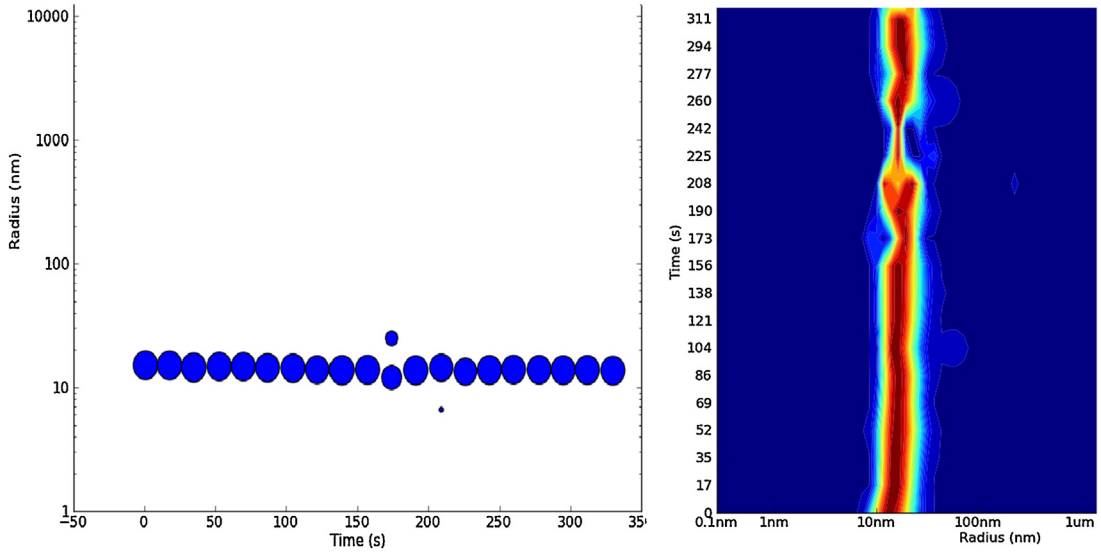

Fig. 3. Dynamic light scattering analysis of VPg (A) a plot (20 scans) of the radius (nm) of the particles in solution as a function of time (s), (B) estimated mean hydrodynamic radius of VPg. The data are the average of 20 measurements.

Effect (NOE) is proportional to the inverse of the sixth power of the distance between two nuclei.

3. Results and discussion

3.1. Virus purification, RNA extraction and cloning of VPg of SBMV

High purity viral particles were obtained from infected bean leaves (Fig. 1), serving as a source of RNA for cDNA synthesis. In this study, the sequence that encodes VPg from SBMV was cloned into the prokaryotic expression vector pET28a. Clones were first screened by PCR analysis and then the expression construct was checked for in-frame fusion by restriction enzyme digestion and DNA sequencing (data not shown).

3.2. Purification and hexahistidine tag removal

Recombinant VPg was purified using Ni-NTA affinity chromatography and incubated with recombinant TEV protease for 16 h at room temperature. The hexahistidine tag and the TEV protease were removed using a second step of Ni-NTA affinity chromatography. The unbound VPg fraction was collected, concentrated to 10 mg/mL and its purity was verified by SDS-PAGE (Fig. 2).

3.3. Dynamic light scattering

Since dynamic light scattering (DLS) provides information about the size distribution of particles in solution, concentrated VPg samples in 20 mM buffer sodium phosphate pH 7.5 and 100 mM NaCl,

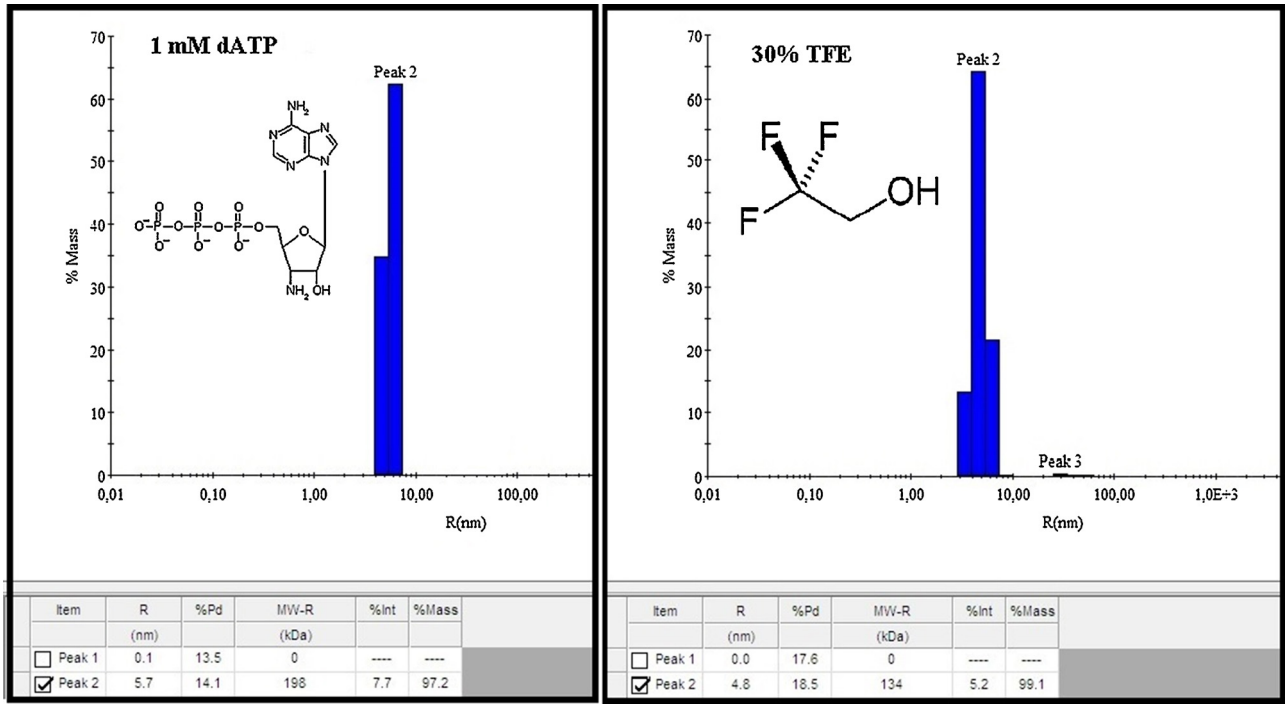

Item	R (nm)	%Pd	MW-R (kDa)	%Int	%Mass
Peak 1	0.1	13.5	0	----	----
Peak 2	5.7	14.1	198	7.7	97.2

Item	R (nm)	%Pd	MW-R (kDa)	%Int	%Mass
Peak 1	0.0	17.6	0	----	----
Peak 2	4.8	18.5	134	5.2	99.1

Fig. 4. Dynamic light scattering analysis of VPg indicating the estimated hydrodynamic radius of VPg is 5 nm in the presence of 1 mM dATP (A) and 30% of TFE (B).

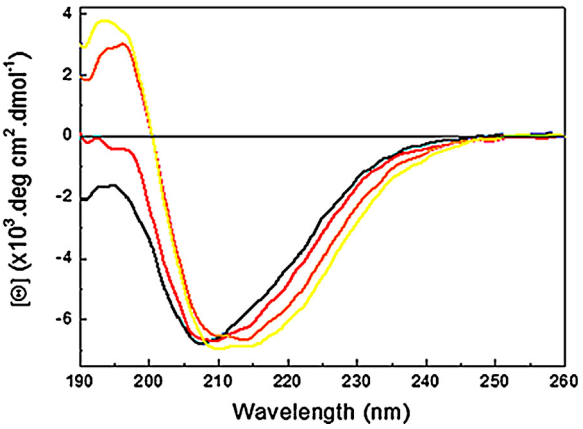

Fig. 5. Far UV-CD spectra of purified VPg in the absence (black line) or in the presence of 10% (red line), 20% (orange line) and 30% (yellow line) of TFE. (For interpretation of the references to colour in this figure legend, the reader is referred to the web version of this article.)

Table 2
Percentages of VPg secondary structure in the absence and presence of TFE.

TFE (%)	α-Helix (%)	β-Sheet (%)	Turn (%)	Random coil (%)
0	8	31	24	37
10	8	33	23	36
20	9	35	23	33
30	15	32	22	31

were present as a monodisperse population (Fig. 3A) with an estimated hydrodynamic radius of 10 nm (Fig. 3B).

The presence of TFE or dATP in solution reduced the estimated hydrodynamic radius of the protein complex from approximately 10 to 5 nm (Figs. 4 and 5) contrary to that observed in the presence of the other additives tested. VPg is an elongated protein and the hydrodynamic radius of 50 Å indicates that it oligomeric under the conditions tested.

3.4. Circular dichroism

Many intrinsically disordered VPgs such as those from poliovirus (genus *Enterovirus*), *Rice yellow mottle virus* (RYMV, genus *Sobemovirus*) and *Lettuce mosaic virus*, *Potato virus A* (LMV and PVA, genus *Potyvirus*) undergo an increase in the percentage of α-helical content in the presence of natural and artificial membranes and also in environments that mimic membranes such as TFE [17].

The VPg CD spectrum in the absence of TFE displayed structural characteristics of an intrinsically disordered protein since its observed minimum was near 205 nm with a negative ellipticity at 190 nm (Fig. 5); the addition of TFE to the buffer solution of VPg induced folding into a predominantly α-helical conformation. The increase in the α-helical content of VPg is based on the positive ellipticity at 190 nm, the shift of the minimum from 205 to 209 nm and increase of the negative ellipticity at 222 nm. Table 2 presents the percentages of secondary structure of VPg obtained using the CONTINLL software. The α-helix propensity of VPg changes with the increment of TFE from 8% to 15% as a result of the stabilization of the α-helix and the random coil percentage decreased from 37% to 31%. Other secondary structural elements underwent only slight changes with the addition of TFE, suggesting that these structures constitute the stable core of VPg.

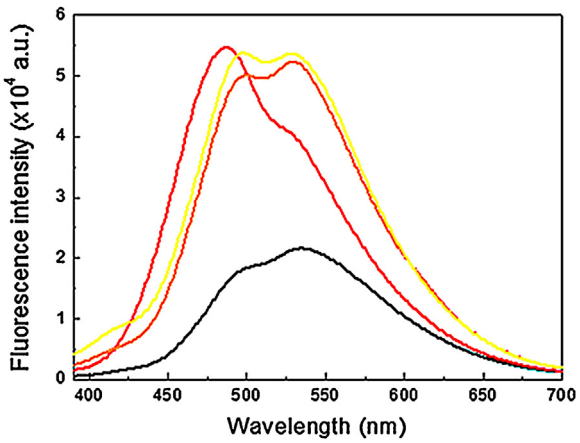

Fig. 6. Fluorescence emission spectra of the binding of ANS to VPg; in the absence (red line) and presence (yellow line) of 30% TFE, and the control ANS emission in phosphate buffer in the absence (black line) and presence (orange line) of 30% TFE in the absence of protein. (For interpretation of the references to colour in this figure legend, the reader is referred to the web version of this article.)

3.5. Binding of probe ANS

The binding of ANS probe to VPg was monitored by steady-state fluorescence spectroscopy. The dye ANS is a probe widely used to investigate the structural changes in proteins and this probe possesses high affinity for the hydrophobic environments in proteins giving rise to significantly enhanced fluorescence with a characteristic blue shift of its emission maximum. Fig. 6 indicates that the fluorescence spectrum of ANS in phosphate buffer increased in the presence of VPg and there was a blue shift of the emission maximum. This increase in the blue shift of the fluorescence emission is characteristic of the binding of ANS probe to unfolded proteins. On the other hand, the emission spectrum of ANS in the presence of VPg plus 30% TFE presented a minor change in relation to its fluorescence in phosphate buffer plus 30% TFE, compared with results obtained in the absence of TFE. This minor change in fluorescence emission of ANS in the buffer with TFE is characteristic of folded proteins. The presence of TFE in the buffer solution likely induced the stabilization of the secondary structure of VPg, since TFE competes for hydrogen bonds with water molecules and thereby inducing the protein to form more hydrogen bond with itself.

3.6. Prediction of intrinsically unstructured/disordered sequence

Using FoldIndex© tool, a predictor of intrinsically disordered regions in the protein sequences, we encountered a probable disordered region of VPg (red sequence in Fig. 7), about 38% of the sequence is structured (green sequence in Fig. 7) in agreement with the circular dichroism experiments which indicated that 38% of the VPg was structured (8% α-helice + 31% de β-strand).

Based on this analysis, we propose, that the conformational changes induced by TFE in VPg of SBMV occur principally in the central and C-terminal regions.

3.7. Nuclear magnetic resonance spectroscopy

For the characterization of the binding interactions between VPg and deoxynucleotides triphosphates (dNTP), the technique of saturation transfer difference NMR (STD-NMR) spectroscopy was used. STD-NMR spectroscopy was first described by Mayer and Meyer [24] and is widely used for ligand screening and affinity evaluation [25,26]. Ligand interactions are detected by selective radiofrequency irradiation of only the protein signals in order to saturate

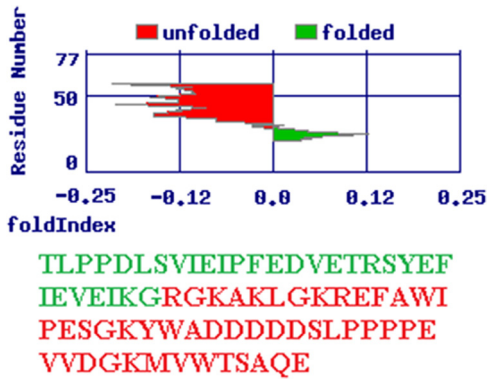

Fig. 7. Bioinformatics based fold index values for VPg of SBMV. The fold index plot indicates the difference between the ordered (green) and disordered (red) regions based on the amino acid composition. The plot predicts extensive unfolded regions in the central and C-terminal regions of the protein. FoldIndex server http://bioportal.weizmann.ac.il/fldbin/finde. (For interpretation of the references to colour in this figure legend, the reader is referred to the web version of this article.)

it, the so-called on-resonance spectrum. Magnetization is then transferred to the ligand via the intermolecular nuclear Overhauser effect and detected if the interaction takes place under the fast chemical exchange condition and interaction of the order of the dissociation constants from a few micromolar to tenths of millimolar may be detected. The key idea behind this technique is that small ligands have positive NOE signals while large macromolecules have negative NOEs. In addition, by comparing the signal intensities in the off-resonance and difference spectra it is possible to evaluate the group epitope mapping, i.e., the ligand atoms that are interacting closely in the protein binding site. Group epitope mapping is considered to be a great advantage of STD-NMR spectroscopy over other techniques used for studying protein–ligand interactions. This information may be used to highlight key differences in the ligand architecture that lead to stable protein interactions.

In the present study, STD-NMR spectra indicated STD effects on the deoxyribose protons C1′, C2′ and C3′ as well as on the nucleobase protons (Fig. 8). Quantifying STD effects as relative STD percentages, the binding epitopes are further assigned. For all dNTPs a significant binding contribution of the deoxyribose moiety, especially C1′, C2′ and C3′ was observed. As C4′ and C5′ showed none or only weak contributions to all dNTP binding due to the greater distance to the protein surface and therefore a significant contribution of the triphosphate moiety is unlikely. Further binding contributions of the dNTPs to VPg are located in the nucleobase moieties, mainly the C8 of adenine and guanine and the C5 for the pyrimidine nucleobases. Interestingly, for dATP the binding contribution of the C8-proton was significantly higher and from the STD effect the most important moiety for binding interactions, compared to the analogue purine base dGTP in which the highest binding contribution is based in the deoxyribose moiety. Because

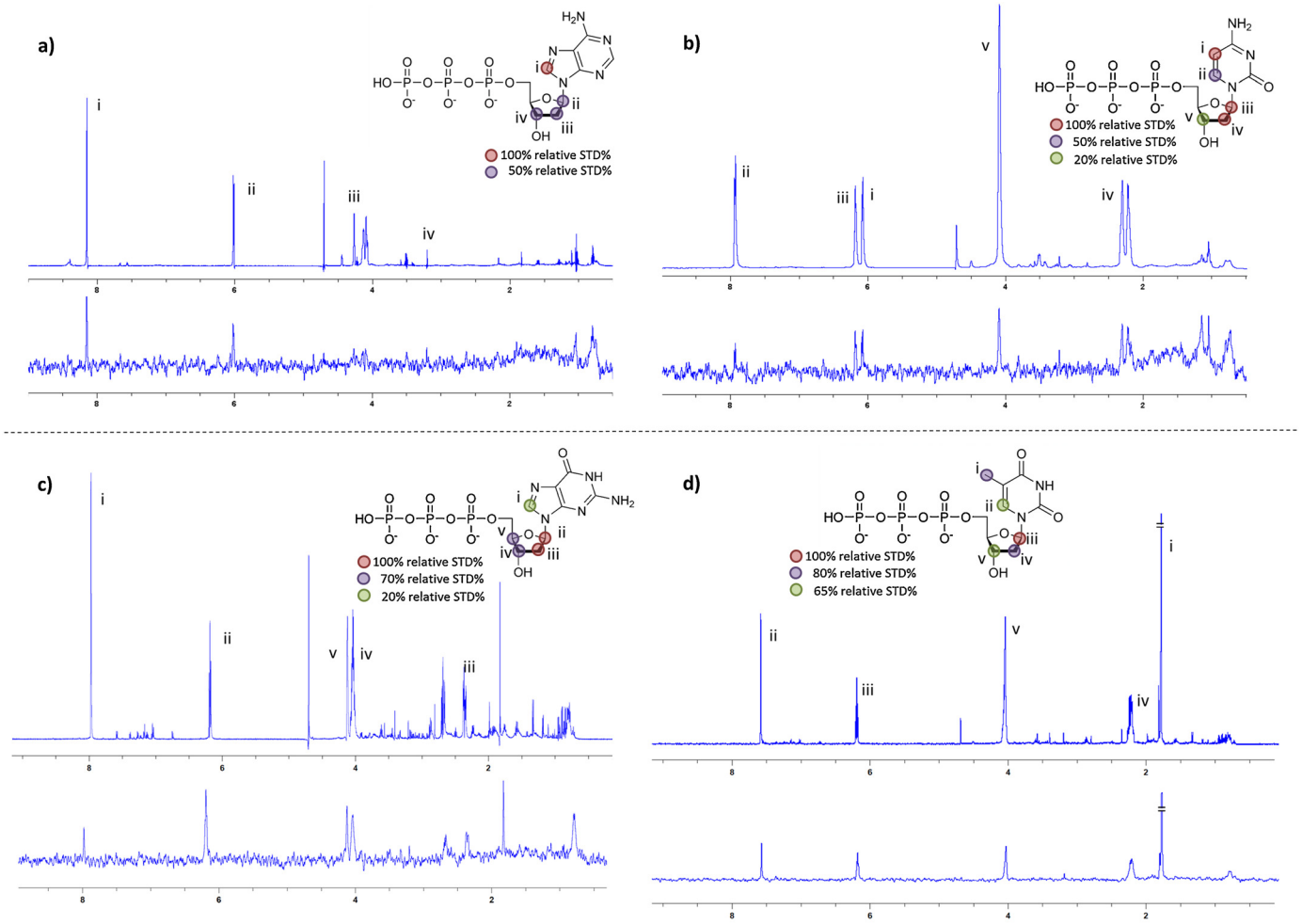

Fig. 8. STD-NMR spectroscopy of VPg and dNTPs. Difference spectra of (a) dATP, (b) dCTP, (c) dGTP and (d) dUTP. The ligand signals are indicated by roman numbers. Relative STD effects are evaluated by percentages compared to the higher individual signal of each spectrum. The CH hydrogens from deoxyribose are associated to 100% STD effect in dCTP, dGTP and dUTP while for dATP they are only 50%; indicating that the interaction of VPg with dATP has greater specificity than to the other dNTPs.

dATP uses the purine motif as the main driving force for binding, we hypothesize that molecular recognition is more specific for this nucleotide. These results are in agreement with the results of Olspert et al. [11] who characterized interactions between threonine of VPg and nucleotides. Also, to further assess the importance of the deoxyribose moiety in the VPg and dATP interaction, STD-NMR experiments were conducted for adenine and a competition experiment between dATP and adenine. Results indicate that the interaction between VPg and adenine still takes place and that VPg has higher affinity towards dATP than towards adenine.

To address the observed effect of the conformational changes as observed by CD spectroscopy, we performed STD NMR experiments for dATP under identical conditions but with the addition of 30% (v/v) TFE and we observed the same pattern as in Fig. 8.

Proteins interact with DNA and RNA via forces which include electrostatic interactions (salt bridges), dipolar interactions (hydrogen bonding), entropic effects (hydrophobic interactions) and dispersion forces (base stacking) whereby this interaction is significantly influenced by their tertiary structures. Beside the phosphodiester bonds, other interactions between nucleic acids and VPg of SBMV may exist and this is not affected by the changes in the percentage of secondary structure. The addition of dATP in VPg solutions does not change the fold of protein as observed with TFE, but results in a decrease of the hydrodynamic radius, suggesting that the binding of this ligand reduces intermolecular interactions. Both the computational and experimental data indicate the possibility that the structure of VPg, especially the central and C-terminal regions, undergo a conformational change when the local hydrophobicity changes.

Author contributions

R.B. Mariutti and A. Ullah expressed and purified the protein. I.P. Caruso performed CD and fluorescence measurements. F.R. De Morais and D. Rehders performed the NMR experiment and R.K. Arni analyzed the data.

Acknowledgments

This research was supported by grants from PROPe-UNESP, CNPq, FAPESP and CAPES (Brazil).

References

[1] I. Goodfellow, Curr. Opin. Virol. 1 (2011) 355–362.
[2] J. Jiang, J.F. Laliberté, Curr. Opin. Virol. 5 (2011) 347–354.
[3] V. Ambros, D. Baltimore, J. Biol. Chem. 253 (1978) 5263–5266.
[4] M. Jaegle, J. Wellink, R. Goldbach, J. Gen. Virol. 68 (1987) 627–632.
[5] N. Nakashima, N. Shibuya, J. Invertebr. Pathol. 92 (2006) 100–104.
[6] E. Sadowy, M. Milner, A.L. Haenni, Adv. Virus Res. 57 (2001) 185–262.
[7] K. Gerber, E. Wimmer, A.V. Paul, J. Virol. 75 (2001) 10969–10978.
[8] R. Anindya, S. Chittori, H.S. Savithri, Virology 336 (2005) 154–162.
[9] P. Puustinen, K. Makinen, J. Biol. Chem. 279 (2004) 38103–38110.
[10] N. Kitamura, C.J. Adler, P.G. Rothberg, J. Martinko, S.G. Nathenson, E. Wimmer, Cell 21 (1980) 295–302.
[11] A. Olspert, L. Arike, L. Peil, E. Truve, FEBS Lett. 585 (2011) 2979–2985.
[12] E.V. Koonin, V.V. Dolja, Crit. Rev. Biochem. Mol. Biol. 28 (1993) 375–430.
[13] A. Olspert, L. Peil, E. Hébrard, D. Fargette, E. Truve, J. Gen. Virol. 92 (2011) 445–452.
[14] J. Mackenzie, Traffic 11 (2005) 967–977.
[15] P. Ahlquist, A.O. Noueiry, W.M. Lee, D.B. Kushner, B.T. Dye, J. Virol. 15 (2003) 8181–8186.
[16] S.A. Whitham, Y. Wang, Curr. Opin. Plant Biol. 7 (2004) 365–371.
[17] R. Grzela, E. Szolajska, C. Ebel, D. Madern, A. Favier, I. Wojtal, W. Zagorski, Biol. Chem. 283 (2008) 213–221.
[18] E. Hébrard, Y. Bessin, T. Michon, S. Longhi, V.N. Uversky, F. Delalande, A.V. Dorsselaer, P. Romero, J. Walter, N. Declerck, D. Fargette, Virol. J. 6 (2009) 23.
[19] K.I. Rantalainen, V.N. Uversky, P. Permi, N. Kalkkinen, A.K. Dunker, Virology 377 (2008) 280–288.
[20] P.S. Satheshkumar, P. Gayathri, K. Prasad, H.S. Savithri, J. Biol. Chem. 280 (2005) 30291–30300.
[21] J. Kim, H. Hwang, H. Min, H. Yun, K. Cho, J.G. Pelton, D.E. Wemmer, C. Lee, Biochem. Biophys. Res. Commun. 459 (2015) 610–616.
[22] A.E. Moreira, J.O. Gaspar, Fitopatol. Bras. 27 (2002) 292–297.
[23] N. Sreerama, R.W. Woody, Anal. Biochem. 282 (2000) 252–260.
[24] M. Mayer, B. Meyer, J. Am. Chem. Soc. 123 (2001) 6108–6117.
[25] M. Pellecchia, I. Bertini, D. Cowburn, C. Dalvit, E. Giralt, W. Jahnke, T.L. James, S.W. Homans, H. Kessler, C. Luchinat, B. Meyer, H. Oschkinat, J. Peng, H. Schwalbe, G. Siegal, Nat. Rev. Drug Discov. 9 (2008) 738–745.
[26] B. Meyer, T. Peters, Angew. Chem. Int. Ed. Engl. 42 (2003) 864–890.